Carbon and nutrient accumulation in tropical mangrove creeks, Amazon region

Christiene R.L. Matos, José Berrêdo, Wilson Machado, Édouard Metzger, Christian Sanders, Marcelo C.L. Cohen

Carbon and nutrients accumulation in tropical mangrove creeks, Amazon region

Christiene R. L. Matos[a,*], José F. Berrêdo[b,*], Wilson Machado[c], Christian J. Sanders[d], Edouard Metzger[e], Marcelo C. L. Cohen[a]

[a]Programa de Pós-Graduação em Geologia e Geoquímica, Universidade Federal do Pará, Belém, Pará, Brazil.

[b]Museu Paraense Emílio Goeldi/MCTIC. Belém, Pará, Brazil.

[c]Programa de Pós-Graduação em Geoquímica, Universidade Federal Fluminense, Niterói, Rio de Janeiro, Brazil.

[d]National Marine Science Centre, Southern Cross University, Coffs Harbour, New South Wales, Australia.

[e]Laboratoire des Bio-Indicateurs Actuels et Fossiles, UMR6112 CNRS LPG-BIAF, Université d'Angers, Angers, France.

*Corresponding authors at: Museu Paraense Emílio Goeldi, Av. Perimetral, 1901 – CEP. 66077-830, Belém – Pará, Brazil.

E-mail addresses: christienematos@hotmail.com (C.R.L. Matos), berredo@museu-goeldi.br (J.F. Berredo), wmachado@geoq.uff.br (W. Machado), christian.sanders@scu.edu.au (C.J. Sanders), edouard.metzger@univ-angers.fr (E. Metzger), mcohen80@hotmail.com (M.C.L. Cohen).

ABSTRACT

The Marapanim River estuary (MRE) is part of the Amazon estuarine system located in northern Brazil, which is characterized as having extensive mangrove forests. Given that previous studies reported CO_2 and CH_4 fluxes from mangrove creeks in this region, here we investigate the

potential organic carbon sequestration of the creek mudflats to get a better understanding of the carbon cycling through these systems. Sediment accumulation rates derived from ^{210}Pb dating indicated that sampled cores represent the previous 24 (± 4) yr. The approximately 24-year total organic carbon (TOC), total nitrogen (TN) and total phosphorus (TP) burial rates were estimated to be 192.5 (± 43.5), 15.3 (± 4.1) and 3.2 (± 0.8) g m^{-2} yr^{-1}, respectively. A binary source mixing model based on carbon stable isotopes ($\delta^{13}C$) revealed that the sedimentary organic matter (OM) is mainly influenced by marine phytoplankton input (49% to 95%). Furthermore, the TOC accumulation rates found here were slightly higher than the global averages estimated for within mangrove forests, suggesting that these unaccounted carbon sinks along creek mudflat environments are relevant for carbon budgets in mangrove-colonized coastal zones. The highest contents, stocks and accumulation rates were found in the tidal creek sediments that are most influenced by nearby mangroves and are more protected than sediments from major river margin. Our results indicate that the creek mudflats play a major role in carbon and nutrients sequestration, directly related to grain size and OM sources.

Keywords: Blue carbon, Organic matter source, Macrotidal estuary, creek mudflat, Brazilian Amazon coast.

1. Introduction

Mangrove forests, along with other vegetated coastal ecosystems such as seagrasses and saltmarshes, are recognized as blue carbon ecosystems due to their capacity to sequester carbon at a far higher rate than terrestrial forests (Nellemann et al., 2009; McLeod et al., 2011). Although mangrove forests occupy <1% of the global coastal area, these ecosystems sequester and store high amounts of organic carbon in plant biomass and sediment, contributing 10 - 15% to coastal sediment carbon storage and exporting 10 - 11% of the particulate terrestrial carbon to the ocean (Jennerjahn

and Ittekkot, 2002; Dittmar et al., 2006; Alongi, 2014). For instance, the carbon stocks in the Amazon mangrove are over twice those of upland evergreen forests and almost 10-fold those of tropical dry forests (Kauffman et al., 2018), which underscores their potential value to mitigating greenhouse gas emissions.

Two important measurements to determining the rate of organic carbon sequestration are the sediment total organic carbon (TOC) content and the sediment accumulation rate (SAR). The first term provides information about the TOC stock sequestered in sediments (Howard et al., 2014). The SAR is used to measure the TOC accumulation rates, which address the question of how much TOC is sequestered in a specified period and quantifies the ongoing sink capacity (Arias-Ortiz et al., 2018). From the ^{238}U decay series, the ^{210}Pb dating method has been an ideal tracer for dating aquatic sediments deposited during the previous 100 years, enabling the determination of TOC accumulation rates in vegetated coastal ecosystems (Smoak et al., 2013; Marchio et al., 2016; Sanders et al.; 2016, Sasmito et al., 2020).

Total organic carbon to total nitrogen ratios TOC/TN ratios, and carbon and nitrogen stable isotope signatures ($\delta^{13}C$ and $\delta^{15}N$) have been widely used as effective geochemical proxies to estimate the relative proportions of terrigenous and marine OM in estuarine and coastal sediments (Lamb et al., 2006; Ranjan et al., 2011; Liu et al., 2015; Vilhena et al., 2018; Kusumaningtyas et al., 2019). Previous studies have shown that the terrestrial OM is preserved, stored and accumulated more efficiently than marine-derived OM in sediments (Hedges et al., 1997; Ranjan et al. 2011; Watanabe and Kuwae, 2015; Kusumaningtyas et al., 2019), due to the selective preservation of refractory OM at the expense of labile components, which is more susceptible to degradation by microorganisms (Hedges et al., 1997; Zonneveld et al., 2010). Therefore, identifying the source of OM is important in evaluating the effectiveness of the mangrove ecosystems as blue carbon sinks, since the variability of the origin of the OM stored in sediments contributes differently to longer-term carbon burial.

Data on the contribution of intertidal creek environments are more limited than mangrove forests as carbon sinks. However, intertidal mudflats situated along mangrove creeks can play an important role in the carbon cycling of tropical land-sea interfaces, such as acting as a conduit for exchanges between mangrove forests and coastal waters. For instance, Call et al. (2019) demonstrated that a mangrove tidal creek in the Amazon region presented large CO_2 and CH_4 fluxes, suggesting that recent global estimates of these fluxes based mostly on data from higher latitudes (exceeding 5°) without considering macrotidal mangrove system, may be underestimated. Moreover, tidal creeks may be more sensitive to land-use changes than open water systems due to a broader connectivity with watersheds, implying that OC accumulation rate changes by up to one order of magnitude in response to urban effluents input (Darrow et al., 2017). Therefore, the balance between carbon export, and sediment burial may present an important conduit to the mangrove and coastal ocean carbon cycle.

The Brazilian coastal region holds, over 960,000 ha, the third-largest mangrove area worldwide (Giri et al., 2011) including the North coast of Brazil (known as the Brazilian Amazon coast) which is considered the largest continuous and best-preserved mangrove forest in the world (Nascimento et al., 2013; Kauffman et al., 2018). The mangroves of the Marapanim River estuary (MRE) are part of this extensive range of mangroves on the Brazilian north coast, which present minimal anthropogenic impact. Mangroves are enormously important in this region as they sustain traditional communities found on the Amazon coast (Fernandes et al., 2018). Information on the biogeochemical cycling of carbon and nutrients in a non-impacted environment is necessary to better understand how potential changes to the mangrove dynamics may impact the carbon and nutrient fluxes between mangrove forests and coastal waters.

The main goal of this study is to obtain a better understanding of the cycling of sedimentary OM in the Marapanim mangrove estuarine system, located in the Brazilian Amazon region. To this aim, the hypothesis that creeks mudflats play an important role as carbon and nutrient sinks, rather

than only act as a conduit for carbon and nutrients cycling in coastal regions, was tested. We analyzed TOC, TN and TP stocks (sediment) and accumulation rates, as well as estimated the sources of OM in unvegetated mudflats situated along mangrove creeks to: 1) characterize the different OM sources, and 2) investigate potential relationships between OM sources and TOC, TN, and TP burial based on accumulation rates. In addition, we characterized the mangrove forest, according to topographical gradients of the tidal flats and vegetation heights, since biogeochemical cycles and carbon budget are also affected by the mangrove structure and environmental conditions (Chambers et al., 2013; Perez et al., 2018; Steinmuller et al., 2020). As such, we suggest that mangrove characteristics should be considered when comparing the biogeochemical data obtained here with other studies.

2. Materials and methods

2.1. Study area

The Marapanim River estuary is part of the Amazon estuarine system in Para, Northern Brazil, between 00º30' to 01º00'S and 47º32' to 47º00'W (Fig. 1a). The main River channel has a funnel form with a length of more than 70 km and a width of 8 km at the mouth (Atlantic Ocean) (Silva et al., 2009). The water of the estuary was extremely mixed as a result of tidal pumping and wave action, with the ocean water penetrating approximately 62 km up the estuary mouth during the dry season and 42 km during the wet season (Berrêdo et al., 2008). This system is dominated by macrotidal regime with semidiurnal tides; their amplitude ranges from 3.5 m during neap tide to over 6 m during spring tides.

The coastal region of Para is characterized by a tropical climate, with a wet season from January to June, and a dry season from July to December, high annual precipitation (2500–3000 mm) and average annual temperature of 27.7 ºC (Martorano et al., 1993). The water temperature of the

estuary varies from 27 to 30 ºC. pH values indicate alkaline conditions during the dry season (7.9 to 8.0) and slight acidic during wet season (5.7 to 6.7). The salinity at low and high fluvial discharge varies from 24 to 3, respectively, in the estuarine channel (Berrêdo et al. 2008).

The estuary is part of the Master Lucindo Marine Extractivist Reserve, a protected Conservation Unit region. The estuary contains 130 km^2 of continuous and pristine mangrove forest (Vilhena et al., 2013). The dominant mangrove species are *Rhizophora* spp., *Avicennia germinans*, and *Laguncularia racemosa*. The trees are tall (up to approximately 35 m, Fig. 1d), generally distributed in mixed forests of *Rhizophora* spp. and *Avicennia germinans*. *Laguncularia racemosa* is found in the mangrove fringe. Saltmarsh vegetation is represented by *Spartina brasiliensis*, which occupies pioneering position in mudflat accretion areas.

The Marapanim catchment extends over an area of 2500 km^2 (Silva et al., 2009), with no industrial development, where about 28,000 people live. Like other Brazilian Amazon coastal cities, the Marapanim city's economy is based mainly on the sustainable use of natural resources, particularly fishing (crabs, shrimps, mollusks and fish), as well as commerce and tourism (Kjerfve and Lacerda, 1993; ICMBio, 2018; Fernandes et al., 2019).

2.2. Acquisition of drone images and processing

Very high resolution (3 cm) images of the study area were obtained using a Drone Phantom 4 DJI (FC 330 digital 4K/12MP camera). The planialtimetric data were processed by the Agisoft Photoscan version 1.6.1 (AgisoftPhotoScan, 2018), and Global Mapper version 19 (GlobalMapper, 2017). Planialtimetric data of ten ground control points were acquired by a smartphone connected to an Antenna Trimble Catalyst with a differential Global Navigation Satellite System (GNSS). A sub-metric correction (± 30 cm), provided by the Trimble website upon payment of a subscription (https://geospatial.trimble.com/catalyst-subscriptions), was applied to the GNSS data. The vegetation

was manually classified by photointerpretation in the Global Mapper Software. *Rhizophora*, *Avicennia*, and *Laguncularia* trees were identified according to color, geometry, and texture of the canopy. This work followed procedures described by the software developer (Agisoft, 2018; "Global Mapper User's Manual," 2020) and adapted for mangrove areas (Cohen et al. 2018, 2019). A detailed description of the data processing can be obtained in the supplementary information section.

2.3. Field sampling

The sediment core collection was conducted during the wet (May 2017) and dry (Sept 2017) seasons. The sampling sites were situated near the mouth (Atlantic Ocean) of the MRE, along a lobular structure, where mangrove vegetation has developed. We compared tidal mangrove creeks (P2 and P3) with the Marapanim River margin (P1), which is located in an area under influence of a nearby sand bar (Fig. 1b).

2.3.1. Sediment

One sediment core was collected from the unvegetated mudflat (devoid of macrophytes) at each site by inserting an acrylic tube (50 cm length) vertically into the substrate during low tide. Immediately after extraction, the sediment core was sectioned at 1-cm depth intervals from the core top to 6 cm depth, then 2-cm intervals until the 20 cm depth, finally at 5-cm intervals until the 35 cm depth. The sub-samples were bagged, preserved on ice and then transported to the laboratory. In addition, pore waters were retrieved using Rhyzon® collectors (Seeberg-Elverfeldt et al., 2005) at the same intervals to the solid phase for salinity analysis. Pore water salinity was measured in situ with a portable refractometer (Atago).

2.3.2. Vegetation and phytoplankton

175 The phytoplankton and vegetation collection was conducted just during the wet (May 2017)
176 season. Approximately 15 fresh leaves of six different adult trees of each dominant mangrove species
177 (*Rhizophora* spp., *Avicennia germinans* and *Laguncularia racemose*) were collected. The leaves were
178 washed in deionized water to remove the adhered sedimentary particles and salt, then the samples
179 were frozen and lyophilized. The phytoplankton samples were collected along the mangrove tidal
180 creek during the flood tides (n=3); horizontal hauls were performed on the water surface (maximal
181 depth 50 cm), using a standard-type plankton mesh, with mesh opening 64 μm. This mesh opening is
182 the most used one in the Amazon estuaries due to the strong local hydrodynamics (Paiva et al., 2006).
183 Each sample was observed in a binocular microscope after it was washed in deionized water and
184 subjected to wet sieving (mesh opening 20 μm) to remove the contaminant particles (leaves and
185 shells) or possible zooplankton predators. Finally, the samples were frozen and lyophilized.
186
187 *2.4. Analyses and data treatment*
188
189 *2.4.1. DBD and Grain size*
190 Dry bulk density (DBD, g cm^{-3}) was determined as the dry sediment weight (g) divided by the
191 initial volume (cm^3). From the original wet section, a portion was taken for grain size analysis. The
192 sediment grain size was determined using a Fritsch particle size meter model Analysette 22, after
193 calcium carbonate and OM removal, and dispersion in sodium hexametaphosphate 4% (Loring and
194 Rantala, 1992). The GRADISTAT 9.1 software (Blott and Pye, 2001) was used for treating results,
195 where the grain size scale was modified from Udden (1914) and Wentworth (1922), with the
196 classification of clay (< 2 μm), silt (2-63 μm) and sand (> 63 μm) are established for these fractions.
197
198 *2.4.2. Elemental and stable isotope analysis*

Carbon and nitrogen stable isotope ratios of phytoplankton, leaves and sediments were measured to identify the sources of OM contributing to the sediments column at each site. A subsample of each core fraction was acidified to remove carbonate material; then it was washed in deionized water, dried (60 °C) and ground to powder before TOC and $\delta^{13}C$ analyses. TN and $\delta^{15}N$ were analyzed in non-acidified subsamples. Isotopic signatures ($\delta^{13}C$ and $\delta^{15}N$) and TOC and TN contents were analyzed using a Leco Flash Elemental Analyser coupled to a Thermo Fisher Delta V isotope ratio mass spectrometer (Thermo Flash EA 1112). Analytical precision was as follows: TOC = 0.1%, TN = 0.1%, $\delta^{13}C$ = 0.1‰, and $\delta^{15}N$ = 0.15‰. Working standards were used (glucose, 10.7 ppt and urea, 41.3 ppt) to calibrate for $\delta^{13}C$. A pair of standards were measured with every 20 samples. These standards were calibrated initially against international absolute standards LSVEC and NIST8542. TP contents in the sediments were determined by colorimetry, according to Grasshoff et al. (1999), following the extraction procedure from Aspila et al. (1976). The results of TOC, TN and TP, expressed in % in this work, were converted to µmol g^{-1} dry weight sediment to calculate individual TOC/TN/TP molar ratios.

2.4.3 Calculation of marine and terrestrial organic matter

The relative proportions of mangrove/terrestrial OM (OM_{terr}) and marine OM (OM_{mar}) in sediment cores were estimated using the two end-member mixing model described in Schultz and Calder (1976):

$$F_{terr} = (\delta^{13}C_{mar} - \delta^{13}C_{sed})/(\delta^{13}C_{mar} - \delta^{13}C_{terr}) \times 100 \text{ and } F_{mar} = 100 - F_{terr} \quad (1)$$

where F_{terr} is the contribution from the mangrove/terrestrial fraction, F_{mar} is the contribution from the marine fraction, $\delta^{13}C_{sed}$ value of the sediment interval, and $\delta^{13}C_{terr}$ and $\delta^{13}C_{mar}$ are the terrestrial and marine end-members value, respectively. We estimated the terrestrial (an average of the plants that

dominate in the Marapanim mangrove) and marine (phytoplankton-derived OM) end-member $\delta^{13}C$ values to be -29.9 ± 1.0 ‰ (n = 18) and -23.9 ± 0.7 ‰ (n = 3), respectively, from our results.

2.4.4. ^{210}Pb dating and rates of organic carbon, nitrogen and phosphorus accumulation

To date sediments, we measured radionuclide activities from the ^{238}U decay series in a high-purity germanium (HPGe) well gamma detector with 40% efficiency coupled to a multichannel analyzer. Sediments at each interval were sealed in gamma tubes for at least three weeks to establish secular equilibrium between ^{226}Ra and its daughter products ^{214}Pb and ^{214}Bi. The ^{210}Pb activities were determined by the direct measurement of 46.5 KeV gamma peaks, while ^{226}Ra activity was calculated averaging its daughters' peaks ^{214}Pb and ^{214}Bi (295.2 KeV) (351.9 KeV) (609.3 KeV) (Sanders et al., 2016). The excess ^{210}Pb ($^{210}Pbex$) activity was estimated by subtracting the ^{226}Ra from the total ^{210}Pb activity. The sediment accumulation rate (SAR) was calculated according to the Constant Initial Concentration (CIC) method as a net downcore decrease in $^{210}Pb_{(ex)}$ activities was noted in all three cores, implying a consistent rate of sedimentation (Appleby and Oldfield, 1992). Accumulation rates and stocks (for 0-35 cm) of TOC, TN and TP were estimated for each depth interval (cm), using values of SAR (cm yr^{-1}), DBD (g cm^{-3}), and TOC, TN as well as TP contents (g g^{-1}), respectively:

Accumulation rates (AR) (g m^{-2} yr^{-1}) = [SAR] x [DBD] x [TOC, TN or TP content] (2)

Stocks (g m^{-2}) = [DBD] x [depth] x [TOC, TN or TP content] (3)

2.4.5. Statistical analysis

Statistical analyses were performed using statistical package PAST version 3.26 (Hammer et al., 2001). One-way analysis of variance (ANOVA) was used to assess the significant difference of a single variable (clay, silt, sand, TOC, TN, TP, $\delta^{13}C$, $\delta^{15}N$) between the sampling sites (P1, P2 and P3) and seasons (wet and dry), with a Tukey HSD post hoc test for distinguishing pairwise relationships among sites. The normality of data distribution was tested using Shapiro-Wilk prior to statistical

249 analysis. When the variables were not normally distributed (clay, silt, sand, TOC, TN and TP), they
250 were log-transformed to fit a normal distribution. Statistical significance at α <0.05 was used for all
251 tests. Principal Components Analysis (PCA) was applied to identify the multivariate relationships
252 between the geochemical variables. Significant factors were selected based on eigenvalues >1. The
253 relation between each pair of variables was measured by Pearson's correlation coefficient. Correlation
254 coefficients greater than 0.5 were considered significant.
255
256 **3. Results**
257
258 *3.1. Mangrove structure*
259
260 The A-B profile (Fig. 1d-e) revealed a young mangrove fringe (1-10 m) mainly represented
261 by *Laguncularia racemosa* in the topographically lowest sector (~1 m above mean sea-level, amsl)
262 of the tidal flat. In an intermediate topography (1 – 2 m amsl) a dense mangrove forest characterized
263 by *Laguncularia racemosa* and *Rhizophora* spp. (10 - 20 m tall) was found. Following the
264 topographical gradient (~2 m amsl) a mixed forest of *Avicennia germinans* and *Rhizophora* spp. is
265 noted (20 - 30 m tall). These trees become taller (25-33 m) in the inner parts of this mangrove forest.
266 The sampling sites P2 and P3 (Fig. 1b) were located in topographically highest areas, inundated only
267 during spring tides, of which sediments are strongly oxidized during the dry season, coexisting with
268 more mature mangroves (15-25 m).
269
270 *3.2. Sediment chronology*
271
272 The log $^{210}Pb_{ex}$ of the sedimentary profiles from the three examined sampling sites were
273 depicted by an almost linear decline with depth (Fig. 2), implying a consistent rate of sedimentation.

Based on the $^{210}Pb_{(ex)}$ profiles, the top 6 cm of the P3 and bottom of the P2 sediment cores were determined to be mixed and therefore, were excluded when calculating SAR. The SAR were calculated as 1.8 (core P1), 1.5 (core P3) and 1.3 (core P2) cm yr^{-1}, respectively (Fig. 2), with a regional mean of 1.5 ± 0.3 cm yr^{-1}. According to the extrapolated $^{210}Pb_{ex}$ - derived age, sediment at the core basis corresponds to an age of about 1997 year in P1 (35 cm), 1989 year in P2 (35 cm) and 1994 in P3 (35 cm).

3.3. Grain size and dry bulk density

The textural composition of the sediments was mostly sand and silt (34–80% of silt, 12–64% of sand) with a low percentage of clay (<10%) (Fig. 3). This textural distribution differs among the three sites ($p<0.05$, Table 2), with the distribution of fine-grained higher at sites P2 and P3 compared with P1 (Fig. 3). The contents of the grain size fractions also showed significant seasonal variations (Table 2), except to silt at P3 and sand at P1 and P2. In general, values of DBD (g cm^{-3}) in the sediment sites increased substantially with the depth (Fig. 3). The highest DBD was found in the P1, exceeding 1.0 g cm^{-3}, where the sedimentary profile graded to predominately sand.

3.4. Elemental and isotopic composition

The values and vertical profiles of elemental and isotopic composition for the sediments, plants and phytoplankton are shown in Table 1 and Fig. 3. Differences in TOC, TN, TP contents of sediments between sampling locations and seasons (except to TN at site P3) were statistically significant (Table 2). The range of TOC was highest at sites P2 (2.28 to 3.84 %) and P3 (2.21 to 3.04 %) compared to P1 (0.53 to 1.91 %). The range of TN was similar to P2 (0.19 to 0.27 %) and P3 (0.19 to 0.26%) compared to P1 (0.04 to 0.17 %). Like TOC and TN, TP contents was much larger in the

P2 (0.028 to 0.052 %) and P3 (0.033 to 0.059 %) than to P1 (0.009 to 0.044%). In all three sites, TOC, TN and TP contents decreased slightly with depth.

The $\delta^{13}C$ values of sediments varied from -26.9 to -24.2‰, with significant difference between sites ($p<0.05$). The downcore $\delta^{13}C$ profile was relatively homogeneous at site P1, without significant difference between seasons ($p>0.05$), with an average of -25.2 ± 0.4‰. However, P2 and P3 showed significant differences between seasons ($p<0.05$), due to results from upper 18 cm, with highest values during dry season, with average of -25.7 ± 0.6‰ and -25.2 ± 0.5‰, compared to wet season, with average of -26.6 ± 0.2‰ and -26.3 ± 0.2‰, respectively.

The $\delta^{15}N$ values of sediments did not differ significantly between seasons ($p>0.05$), but differed significantly between sites ($p<0.05$). The $\delta^{15}N$ values ranged from 5.1 to 8.4‰, with an average of 6.1 ± 0.8‰ to P1, 5.9 ± 0.6‰ to P2 and 6.5 ± 0.3‰ to P3. Downcore profiles of $\delta^{15}N$ showed a small increase with depth, excepted for site P1 that showed oscillations and no tendency with depth, with a peak at 14 cm.

Differences in TOC/TN molar ratios between sampling locations and seasons were statistically significant (Table 2), varying from 12 to 18.5, with an average of 15.3 ± 1.3 to P1, 15.6 ± 1.3 to P2 and 13.7 ± 0.8 to P3. Downcore profiles of TOC/TN showed a small increase with the depth at all sites. The TN/TP molar ratios in sediments were not significantly different in terms of spatial variability ($p>0.05$), but were significantly different seasonally, with highest ratios in the wet season, varying from 8.3 to 13.3, compared to dry season, that varied from 2.9 to 11.8.

The $\delta^{13}C$ values of *Rhizophora* spp., *Avicennia germinans* and *Laguncularia racemosa* leaves were similar and ranged from -31.8 to -28.2‰ (29.8 ± 1.0 ‰), which is within the range of C_3 terrestrial plants. The $\delta^{15}N$ and TOC/TN values varied slightly from species to species from 1.7 to 6.4‰ (4.4 ± 1.3 ‰) and from 30.0 to 40.1 (34.0 ± 3.2), respectively. The phytoplankton presented $\delta^{13}C$ values from −24.4 to −23.4‰ (23.9 ± 0.7 ‰), $\delta^{15}N$ from 3.2 to 3.7‰ (3.4 ± 0.4 ‰), and TOC/TN from 6.9 to 7.2 (7.1 ± 0.2).

3.5 Principal Component Analysis (PCA)

The significant components (ie., eigenvalue >1) loading matrix of PCA are listed in Table 3. The PCA (Fig. 4) showed that the first two components together explained 74.5% of the data variation. The first component (PC1) accounted for the largest proportion with 61.7% of the total variance. It showed significant positive loading (> 0.5) for TN, TOC, TP, silt and clay, and negative loading of sand and $\delta^{13}C$. The first component explained the variations between the sites, separating the site P1 from P2 and P3 due to its high sand content (Fig. 4a). This component also gives strong evidence of TOC, TN and TP increase with increase of silt and clay, with the highest TOC, TN and TP contents for P2 and P3 (Fig 4b). The second component (PC2) explained 12.9 % of the total variance and showed significant loading only for $\delta^{15}N$.

3.6. Proportions of organic matter sources

The proportions of terrestrial (OM_{terr}) and marine (OM_{mar}) OM sources were derived from the $\delta^{13}C$ data and Eq. (1). Downcore profiles of OM_{mar} and OM_{terr} remained relatively constant throughout the sediment columns during the wet season, but during the dry season an increase in marine input in the upper layers (< 18 cm) was observed at sites P2 and P3 (Fig. 3). Relatively high proportions of OM_{mar} were observed at all sites in both wet and dry seasons. Overall, OM_{mar} varied from 49.1 to 95.2% and OM_{terr} from 4.8 to 50.9% (Table 1). In the wet season, OM_{mar} contribution was highest in the site P1 (76.4 %) compared to sites P2 (54.5 %) and P3 (60 %). During dry season, OM_{mar} increased to 79.6, 69 and 78 % at sites P1, P2 and P3, respectively.

3.7. Stocks and accumulation rates

The TOC, TN and TP accumulation rates and stocks are shown in Fig. 5 and Table 4. The TOC, TN, and TP accumulation rates were estimated from SAR, DBD and TOC, TN and TP content results (Eq. (2)). The downcore sediment densities along with the TOC, TN and TP contents were used to determine stocks (Eq. (3)), the stocks were calculated to 30 cm sediment depth for the three sampling sites. The TOC, TN and TP accumulation rates showed significant site-difference ($p<0.05$), with a regional mean of 192.5 ± 50.6 g m^{-2} y^{-1} for TOC, 15.3 ± 4.3 g m^{-2} y^{-1} for TP and 3.2 ± 1.0 for TP. The highest TOC, TN, and TP accumulation rates were measured at sites P2 (C: 218.7, N: 16.4, and P: 3.1 g m^{-2} yr^{-1}) and P3 (C: 215.8, N: 18.4, and P: 3.9 g m^{-2} yr^{-1}) and the lowest were measured at site P1 (C: 143.2, N: 11.0, and P: 2.7 g m^{-2} yr^{-1}). The TOC, TN and TP stocks also differed significantly among the three sites ($p<0.05$), with a regional mean of 3811 ± 1389 g m^{-2} for TOC, 296 ± 109 g m^{-2} for TN and 58 ± 15 g m^{-2} for TP. Similarly, the TOC, TN and TP stocks were higher at sites P2 (C: 5217.8, N: 386.3, P: 64.9 g m^{-2}) and P3 (C: 3878.6, N: 325.8, P: 55.4 g m^{-2}) than P1 (C: 2337.5, N: 177.1, P: 17.1 g m^{-2}).

4. Discussion

4.1. Sedimentary composition

The mudflat sediments were found to be mainly composed of a mixture containing silt and sand, reflecting a moderately high energetic environment, influenced by tide and fluvial process. The low hydrodynamics flow in the mangrove creeks (P2 and P3) likely caused an increase in the deposition of fine sediments. However, the MRE margin, where P1 was collected, appears to be more affected by tidal currents. In addition, the P1 site is located closer to the sand bar that likely contributed to the increase of fine sand in the sedimentary profile at this study site.

374 The spatial variations in the grain size distribution of the mudflat sediments play an important
375 role in controlling the OM content. Silt and clay had positive strong to moderate correlation with
376 TOC, TN and TP contents (r varied from 0.52 to 0.81). The first component of the PCA also indicated
377 strong evidence that TOC, TN and TP increase as the silt and clay increase, with the highest TOC,
378 TN and TP contents for P2 and P3 (Fig 4a-b). Generally, fine-grained (silt + clay) sediments have
379 higher %TOC than coarse sediments (Canfield, 1994), such relationships may be attributed to the
380 fine-grained sediments which have large specific surface areas that provide higher capacity to adsorb
381 OM (Loring and Rantala, 1992; Mayer, 1994).
382 The TOC and TN contents measured in the sediments during the present study are comparable
383 to those reported in the adjacent coastal areas (Kauffman et al. 2018; Vilhena et al., 2018) and the TP
384 contents are within the global average for mangrove (0.01–0.16%; Alongi et al., 1992). The gradual
385 decrease of TOC, TN and TP content with depth in all cores likely reflect the decomposition of OM
386 by microorganisms as noted in other systems (Kristensen et al., 2008) or a general increase in the OM
387 content with time. The significant positive correlation between TOC and TN (r= 0.96) and TP (r=
388 0.83) in the sediments indicate that the nitrogen and phosphorous in the samples are predominantly
389 associated with the organic fraction.
390 The TOC/TN/TP molar ratios in sediments were not significantly different in terms of spatial
391 variability, but were significantly different seasonally: 171:11:1 in the wet season and 71:5:1 in the
392 dry season. In both cases the TOC/TN/TP was different from the phytoplankton sources (Redfield:
393 106:16:1), with TN/TP ratios below 16 that suggest nitrogen to be the limiting factor for
394 phytoplankton growth in these systems. This seasonal variation may be related to the diagenesis of
395 OM. Higher TOC/TN molar ratios in wet than dry season indicate a greater contribution from OM of
396 terrestrial origin, which is more refractory, during the wet season.
397
398 *4.2. Sources of sedimentary organic matter*

399

400 Diff erent sources of OM often exhibit distinct elemental (carbon and nitrogen) and/or isotopic
401 signatures ($\delta^{13}C$ and $\delta^{15}N$), representing useful indicators to quantify their relative contribution to the
402 sedimentary OM. For example, C_3 plants are assumed to have TOC/TN > 12 (Meyers, 1997), $\delta^{13}C$
403 between −32‰ and −21‰ (Deines, 1980) and $\delta^{15}N$ around 0.4 ± 0.9‰ (Peterson and Howard, 1987),
404 while marine-derived OM is characterized by TOC/TN between 5 and 7 (Redfield et al., 1963), $\delta^{13}C$
405 from −16‰ to −23‰ (Meyers, 1994) and $\delta^{15}N$ around 8.6 ±1.0‰ (Peterson and Howard, 1987).
406 The potential sources to the sedimentary OM pool in mangrove-estuarine ecosystems can be
407 upland forest and mangrove tissues (fresh leaf, stem, root, and litter), soils from river flow, aquatic
408 macrophytes, microphytobenthos, and phytoplankton (Bouillon et al. 2008; Sasmito et al., 2020).
409 Some studies have also identified the presence of microphytobenthos as a potential source of OM in
410 mudflats (Gontharet et al., 2014; Gorman et al., 2020), when microphytobenthos layers are visually
411 detectable and thick enough to be sampled and separated from the sediments. However, the presence
412 of microphytobenthos was not visually detectable in our sampling sites, therefore prohibiting the
413 separation and analyses of a potential benthic microalgae endmember. Saltmarsh vegetation (*Spartina*
414 spp.), dominated by C_4 plants, can be found at the mudflats along MRE. However, given that *Spartina*
415 spp. and their sediments have enriched $\delta^{13}C$ signature, ranging from -14 to -12 ‰ and -18 to -14 ‰,
416 respectively (Currin et al., 1995; Kemp et al., 2020, and references therein), the depleted $\delta^{13}C$ values
417 found in sediment samples suggests that *Spartina* spp. is not a major contributor of OM to the studied
418 mudflat sediments. Therefore, we assumed mangrove plants and phytoplankton as the principal OM
419 sources to the mudflats along MRE.
420 The $\delta^{13}C$ values of mangrove leaves (-31.8 to -28.2‰) are consistent with previously
421 published results from other mangrove-estuarine ecosystems (Bouillon et al., 2008; Prasad and
422 Ramanathan 2009; Ranjan et al., 2011; Vilhena et al., 2018). The $\delta^{13}C$ and $\delta^{15}N$ values and TOC/TN
423 molar ratio of phytoplankton (average of -23.9 ± 0.7‰, 3.4 ± 0.4‰ and 7.1 ± 0.2, respectively), which

424 we extracted along the studied tidal creek, are close to the marine phytoplankton values. The $\delta^{13}C$
425 values are also similar to the reported value for marine DOC (average -23.7‰) extracted from
426 Atlantic deep water in the adjacent study area (Dittmar et al., 2006).

427 The $\delta^{13}C$ (-26.9 to 24.2‰) versus TOC/TN (12.0 to 18.5) (Fig. 6) of the sedimentary OM
428 suggests a mixture of sources contributing to the sedimentary OM pool, with a higher contribution of
429 marine phytoplankton ($\delta^{13}C$: -23.9 ± 0.7 ‰, TOC/TN: 7.1 ± 0.2) than mangrove-derived OM ($\delta^{13}C$:
430 -29.8 ± 1.0‰, TOC/TN: 34 ± 3.1). The $\delta^{15}N$ values of sediments (5.2 – 8.4‰, average of 6.2‰) are
431 within a typical range of aquatic OM produced from assimilation of the nitrate pool. The slight
432 increase of $\delta^{15}N$ values and TOC/TN molar ratios with depth, with exception to site P1 in the wet
433 season, suggests anaerobic microbial degradation of OM in the deep reducing sediments (Meyers,
434 2003; Routh et al., 2009; Jennerjahn, 2012; Prasad et al., 2017). The peak of $\delta^{15}N$ at 14 cm in the site
435 P1 during wet season could reflect an event provoked by input from a phytoplankton bloom or
436 accumulation of allochthonous material deposited during and after a rainfall.

437 The consistently similar values of the $\delta^{13}C$ throughout the sediment column suggest that the
438 source of the depositional OM has been invariable during the past ~25 years at site P1. However, at
439 sites P2 and P3, the enrichment of $\delta^{13}C$, during the dry season compared to wet season, indicated a
440 shift in OM source, because the decomposition of OM usually does not cause a significant enrichment
441 of $\delta^{13}C$ (Saintilan et al., 2013), and isotopic fractionation during the decomposition is <3‰. This shift
442 in OM accumulation may be due to an increase in marine input in the upper layer (< 18 cm), likely
443 associated with a larger sediment mixing provoked by bioturbation in the surface sediments, as the
444 $\delta^{13}C$ values were relatively similar along the bottom layers.

445 The difference in OM source for terrestrial/mangrove C_3 plants ($\delta^{13}C$: -29.8 ± 1.0 ‰) vs.
446 marine phytoplankton ($\delta^{13}C$: -23.9 ± 0.7 ‰) is distinct and hence, suitable for indicating the OM
447 sources in the study area. However, $\delta^{15}N$ values and TOC/TN molar ratios can be unreliable because
448 these are influenced by diagenetic alterations (Prahl et al., 1997). Additionally, $\delta^{13}C$ did not show

449 significant positive correlations with $\delta^{15}N$ ($r < 0.08$) and TOC/TN molar ratios ($r < 0.05$) in either the
450 wet or dry season. Therefore, only $\delta^{13}C$ was used for the quantification analysis of OM. Based on the
451 assumption of differing OM source input to the mudflat sediments, the end-member mixing model of
452 terrestrial and marine OM showed that the contribution of OM sources varied between sites and
453 seasons (Fig 3, Table 1).

454 The OM_{mar} predominated in the studied sites likely due to the positioning of the sampling
455 sites, which are situated near the mouth of the MRE (Atlantic Ocean). During the wet season (pore
456 water salinity: 4-20), the OM_{mar} contribution was highest in the mudflat sediment from MRE margin
457 (P1: 76.4 %) compared to the mangrove tidal creeks (P2: 54.5, P3: 60 %). During the dry season (pore
458 water salinity: 18-25), due to less dilution from Marapanim River discharge, the influence of salt
459 water is greater, thereby increasing the contribution of OM_{mar} by up to 18 % (P1: 79.6, P2: 69 and
460 P3: 78 %). Overall, the downcore profiles of OM_{mar} and OM_{terr} remained relatively constant
461 throughout the sediment columns during the wet season, but during the dry season an increase in
462 marine input in the upper layers (< 18 cm) is noted at sites P2 and P3 (Fig. 3).

463

464 *4.3. Carbon and nutrients accumulation rates and stocks*

465

466 The TOC, TN and TP accumulation rates and stocks showed differences between the sites
467 (Table 2, Fig. 5). The highest stocks and accumulation rates were found in the mudflat sediment from
468 mangrove tidal creek (P2 and P3) compared to the MRE margin (P1). Two factors may cause these
469 differences. Firstly, although site P1 presented the highest sedimentation rate (Fig. 2) and highest
470 density (Fig. 3), it is composed of >50% sand content with lower TOC, TN and TP contents compared
471 to the sites P2 and P3. Previous studies indicated that OM preservation is often enhanced by the large
472 surface area of fine-grained sediments, and the low energy associated with slack water deposits

(Mayer, 1994; Keil et al. 1994). Sites P2 and P3 are protected from the direct impact of tidal energy and waves, as compared to site P1 that is located in the MRE margin and close to a sand bar.

The other factor is that the efficiency of OM storage in the mudflat sediments is also dependent on the origin of OM (Saintilan et al., 2013; Watanabe and Kuwae, 2015; Kusumaningtyas et al., 2019). OM proportions in our simple end-member mixing model indicated that 49-95% of OM contribution is from marine OM. The slight increase in fluxes of terrestrial OM along the mangrove tidal creek sites (P2 and P3, Table 1) contributed to higher TOC, TN and TP accumulation rates and stocks than those seen along the MRE margin (P1). These results were corroborated with previous studies, which indicated the terrestrial OM is preserved more efficiently than phytoplankton-derived OM in estuarine sediments (Hedges et al., 1997).

The average TOC accumulation rate (TOC AR) calculated in the studied mudflats was slightly higher (192.5 ± 43.5 g C m^{-2} yr^{-1}) than the global average in conserved mangrove (170 g C m^{-2} yr^{-1}, Perez et al., 2018) and the current global average for mangrove ecosystems (179.6 g C m^{-2} yr^{-1}, Alongi, 2020). Higher rates of 555 g C m^{-2} yr^{-1} were measured in other tropical mudflat in Piraquê-Açu estuary, Brazil, supported by high SAR (1.8 cm yr^{-1}, Bernadino et al., 2020). In contrast, lower carbon accumulation rates were reported in subtropical microtidal creeks systems. For example, Marchio et al. (2016) evidenced TOC AR of 162 g C m^{-2} yr^{-1} in Southwest Florida, and Santos et al. (2019) observed TOC AR of 63 g C m^{-2} yr^{-1} in a tidal creek in Evans Head, Australia. However, according Perez et al. (2018), the distribution of TOC AR within the forests and adjacent sites (margin and mudflat environments) of mangrove ecosystems exhibited non-significant differences among regions, as variations are influenced by a combination of many local factors (e.g. geomorphology, vegetation cover, flooding frequency, hydrological regime and anthropogenic influence).

The average TN and TP accumulation rates were also high (TN: 15.3 g m^{-2} yr^{-1} and TP: 3.2 g m^{-2} yr^{-1}; Table 4) when compared to the global average of anthropogenically non-impacted mangroves (TN: 8.9 g m^{-2} yr^{-1} and TP: 0.5 g m^{-2} yr^{-1}, Breithaupt et al., 2014). Similar to our study,

Bernadino et al. (2020) measured high TN accumulation rates of 27.9 g m^{-2} yr^{-1} in a conserved mudflat in Piraquê-Açu estuary. OM enriched in nutrients may be expected to decompose faster and to a larger extent than nutrient-depleted OM (Kristensen and Hansen, 1995; McGlathery et al., 2007). Thereby, the capacity to sequester OC may decrease with the increase of TN and TP burial rates (Breithaupt et al., 2014). However, in our study area TOC AR were higher in the sites with higher TN and TP AR. Similarly, TOC stocks were higher in the sites with higher TN and TP stocks (Table 4).

Due to the relatively shallow sediment depth (30 cm) used in our study, it is difficult to directly compare our results with those from other studies which usually assess sediment stocks based on deeper cores (e.g., ≥100 cm, Howard et al., 2014). However, we found some studies similar to ours with more superficial sampling. Our TOC stocks ranged from 2333 to 5218 g C m^{-2} (average of 3811 g C m^{-2}), which is similar those mudflat of West Papua, Indonesia (in the top 50 cm, 6200 g C m^{-2}; Sasmito et al., 2020), Araçá Bay, Brazil (in the top 20 cm, range from 1700 to 2200 g C m^{-2}; Gorman et al., 2020), and for unvegetated mudflats of China (in the top 50 cm, 4808 g C m^{-2}; Feng et al., 2019). Comparing our stocks results with the values found in other Amazon mangroves sediments (in the top 30 cm) (supplementary information in Kauffman et al., 2018), our values are within the range of 3430 – 6230 g C m^{-2}, except at site P1 that was relatively lower (2337 ± 279 g C m^{-2}), which can be attributed to coarse textured sediments. These results suggest that mudflat along tidal creeks also have a high potential for organic carbon storage compared to vegetated habitats such as mangrove forests.

Few studies have assessed nitrogen and phosphorus stocks in mangrove and mudflat sediments. Feng et al. (2017) measured TN and TP stocks in an unvegetated mudflat of China (in the top 40 cm). Their average of TN stock of ~290 g N m^{-2} is comparable to 296 ± 109 g N m^{-2} (Table 4) in our study, but TP stock of ~150 g P m^{-2} is higher than what we found of 58 ± 15 g P m^{-2} (Table 4). Saderne et al. (2020) measured TN and TP stocks in mangrove sediments (in the top 20 cm) in the central Red Sea (99 g N m^{-2} and 70 g P m^{-2}) and along the Gulf coast of Saudi Arabia (223 g N m^{-2}

and 32.8 g P m^{-2}), where TN and TP stocks in the Gulf were quite comparable to what is presented here, but TN stocks were at least twofold higher in the Gulf compared to the Red Sea, while TP stocks were a maximum of 1.2 times higher in Red Sea. Perez et al. (2017) observed in a conserved mangrove forest in New Zealand estuary TN stock between 400 and 500 g N m^{-2}, in the top 40 cm, which is slightly higher than our values. In contrast, Ray et al. (2014) and Ray et al. (2017) measured the TN and TP stocks, respectively, in the top 60 cm sediment in the Indian Sundarban mangrove and found an average of 4.2 g N m^{-2} and 0.4 g P m^{-2}, which are lower than we found (58 ± 15 g P m^{-2}, Table 4), like as a result of the TN and TP conserved in the living biomass.

The capacity to sequester and store OM in the studied creek mudflats likely reflects the SAR (1.5 ± 0.3 cm yr^{-1}), which is higher than the global average in conserved mangrove (0.36 ± cm yr^{-1}; Perez et al., 2018) and the current global average (0.77 cm yr^{-1}; Breithaupt et al., 2012). This high SAR is supported by strong interaction between the river stream and the tides that characterize this environment, being close to the highest global accumulation rates in the mangrove forest (Breithaupt et al. 2012; Kusumaningtyas et al., 2019) and mudflat (Bernadino et al., 2020). In general, the sedimentation rate is considered as a driving factor controlling the OM burial efficiency (Canfield, 1994). Although the sedimentary OM with a high proportion of marine origin tends to be more susceptible to decomposition, sites with high sedimentation rates contribute significantly to preserve OM (Hedges and Keil, 1995; Canfield et al., 2005). In addition, it should be noted that the studied mangrove area is densely inhabited by *Rhizophora*, *Avicennia* and *Laguncularia* trees, with heights up to 33 m. This probably reflects a high productivity that provided a large supply of mangrove litter and dead roots to the mangrove creeks through tidal exchange.

Recently, Call et al. (2019) demonstrated that a mangrove tidal creek in Amazon presented large CO_2 and CH_4 fluxes from a nearby mangrove tidal creek. However, our results indicate that the Amazon mangrove creeks are also sites that accumulate considerable amounts of organic carbon (Fig. 7). For example, the total mudflat area in the tidal creek catchment of this study was near 0.5 km^2

(Fig. 1c), and considering an average of the TOC accumulation rates between the three study sites, we estimate that a total of 96 kg TOC yr^{-1} is sequestered in these creeks catchment. This suggests a previously unaccounted carbon sink in creek environments that are relevant to the carbon budgets along mangrove-colonized coastal zones. Therefore, mangrove tidal creeks can play an important role in the carbon cycling in tropical land-sea interfaces more than just acting as a conduit for exchanges between mangrove forests and coastal waters.

Considering global average in conserved mangrove of 170 g C m^{-2} yr^{-1} (Perez et al., 2018) and the mangrove forest area within the catchment of this study was 7,638,368 m^2, we estimate that a total of 1299 t TOC yr^{-1} is sequestered in these mangrove soils. Thus, the creek mudflat area accumulates around 0.007% of what would be estimated for the mangrove forest soils. Carbon dioxide emissions at the water–air interface were 2794 ± 2072 g m^{-2} yr^{-1} (174 ± 129 mmol m^{-2} d^{-1}) from a nearby mangrove tidal creek (Call et al., 2019). Using our creek mudflat area (0.5 km^2), CO_2 emissions would be 1397 kg C-CO_2 yr^{-1}, while total mudflat sediment carbon burial would be 96.3 kg yr^{-1}. Therefore, sediment carbon sequestration in this system may offset < 7.0 % of the aquatic CO_2 emissions.

5. Conclusion

This study investigated the recent (24 ± 4 years) carbon and nutrient accumulation rates and stocks in intertidal mudflats situated along mangrove creeks within the Brazilian Amazon coast. Even though marine OM was predominant along our study sites (49% to 95%), fine-grained sediments and higher terrestrial OM input, a product of a dense and tall mangroves trees, contributed to higher rates of TOC, TN, and TP accumulation and stocks in the mangrove tidal creeks (P2 and P3) compared to the Marapanim River estuary margin (P1). The capacity to sequester and store TOC also increased with increases in TN and TP burial rates and stocks. Due to the high sedimentation rates (1.5 ± 0.3

573 cm yr^{-1}), the TOC (192.5 ± 43.5), TN (15.3 ± 4.1), and TP (3.2 ± 0.8) accumulation rates found here
574 were slightly higher than the global averages estimated for mangrove forest sediments. The potential
575 of intertidal mudflats to sequester OC suggests that the creek environments are unaccounted carbon
576 sinks and are relevant in terms of carbon budgets in mangrove-colonized coastal zones.
577
578 **Acknowledgements**
579
580 The authors thank the research grants from the Brazilian Ministry of Education (CAPES) and
581 Brazilian Research Council (CNPq) to C.R.L. Matos and W. Machado. C.J. Sanders is supported by
582 Australian Research Council (DE160100443) and E. Metzger by CNRS-EC2CO project Vubleu.
583
584 **References**
585
586 AgisoftPhotoScan, 2018. AgiSoft PhotoScan Professional. Version 1.4.5. Agisoft LLC. St.
587 Petersburg, Russia. Retrieved from http://www.agisoft.com/downloads/installer/.
588
589 Alongi, D.M., Boto, K.G., Robertson, A.I., 1992. Nitrogen and phosphorus cycles, in: Robertson,
590 A.I., Alongi, D.M. (Eds.), Tropical Mangrove Ecosystems. Coastal and Estuarine Studies. American
591 Geophysical Union, Washington, DC, pp. 251–292. https://doi.org/10.1029/ce041p0251.
592
593 Alongi, D.M., 2014. Carbon cycling and storage in mangrove forests. Annu. Rev. Mar. Sci. 6, 195–
594 219. https://doi.org/10.1146/annurev-marine-010213-135020.
595
596 Alongi, D.M., 2020. Global Significance of Mangrove Blue Carbon in Climate Change Mitigation
597 (Version 1). Sci, 2, 57.
598
599 Appleby, P.G., Oldfield, F., 1992. Application of lead-210 to sedimentation studies, in:
600 Ivanovich, M., Harmon, S. (Eds.), Uranium Series Disequilibrium: Application to
601 Earth, Marine and Environmental Science, second ed. Oxford Science Publications, pp. 731-783.
602

603 Arias-Ortiz, A., Masqué, P., Garcia-Orellana, J., Serrano, O., Mazarrasa, I., Marbà, N., Lovelock,
604 C.E., Lavery, P.S., Duarte, C.M., 2018. Reviews and syntheses: ^{210}Pb-derived sediment and carbon
605 accumulation rates in vegetated coastal ecosystems – setting the record straight. Biogeosciences 15,
606 6791–6818. https://doi.org/10.5194/bg-15-6791-2018.
607
608 Aspila, K.L., Agemian, H., Chau, A.S.Y., 1976. A semi-automated method for the determination of
609 inorganic, organic and total phosphate in sediments. Analyst 101, 187–197. https://doi.org/
610 10.1039/AN9760100187.
611
612 Bernardino, A.F., Sanders, C.J., Bissoli, L.B., de O. Gomes, L.E., Kauffman, J.B., Ferreira, T.O.,
613 2020. Land use impacts on benthic bioturbation potential and carbon burial in Brazilian mangrove
614 ecosystems. Limnol. Oceanogr. 9999, 1-11. http://dx.doi.org/10.1002/lno.11458.
615
616 Berrêdo, J.F., Costa, M.L., Progene, M.P.S., 2008. Efeitos das variações sazonais do clima tropical
617 úmido sobre as águas e sedimentos de manguezais do estuário do rio Marapanim, costa nordeste do
618 Estado do Pará. Acta Amazônica 38, 473-482. http://dx.doi.org/10.1590/S0044-
619 59672008000300012.
620
621 Blott, S.J., Pye, K., 2001. GRADISTAT: a grain size distribution and statistics package for the
622 analysis of unconsolidated sediments. Earth Surface Processes and Landforms 26, 1237-1248.
623 https://doi.org/10.1002/esp.261.
624
625 Bouillon, S., Connolly, R.M., Lee, S.Y., 2008. Organic matter exchange and cycling in mangrove
626 ecosystems: Recent insights from stable isotope studies. Journal of Sea Research, 59, 44-58,
627 https://doi.org/10.1016/j.seares.2007.05.001.
628
629 Breithaupt, J.L., Smoak, J.M., Smith, T.J., Sanders, C.J., Hoare, A., 2012. Organic carbon burial rates
630 in mangrove sediments: strengthening the global budget. Global Biogeochem. Cycles 26.
631 https://doi.org/10.1029/2012gb004375.
632
633 Breithaupt, J.L., Smoak, J.M., Smith, T.J., Sanders, C.J., 2014. Temporal variability of carbon and
634 nutrient burial, sediment accretion, and mass accumulation over the past century in a carbonate

635 platform mangrove forest of the Florida Everglades. J. Geophys. Res. Biogeosci. 119, 2032–2048.
636 https://doi.org/10.1002/2014JG002715.
637
638 Call, M., Santos, I.R., Dittmar, T., Rezende, C.E., Asp, N.E., Maher, D.T., 2019. High pore-water
639 derived CO_2 and CH_4 emissions from a macro-tidal mangrove creek in the Amazon region.
640 Geochimica et Cosmochimica Acta 247, 106–120. https://doi.org/10.1016/j.gca.2018.12.029.
641
642 Canfield, D.E., 1994. Factors influencing organic carbon preservation in marine
643 sediments. Chem. Geol. 114, 315-329. https://doi.org/10.1016/0009-2541(94)90061-2.
644
645 Canfield, D.E., Kristensen, E., Thamdrup, B., 2005. Heterotrophic Carbon Metabolism. Aquatic
646 geomicrobiology: Advances Marrine Biology 48, 129-166. https://doi.org/10.1016/S0065-
647 2881(05)48005-0.
648
649 Chambers, L.G., Davis, S.E., Troxler, T., Boyer, J.N., Downey-Wall, A., Scinto, L.J., 2013.
650 Biogeochemical effects of simulated sea level rise on carbon loss in an Everglades mangrove peat
651 soil. Hydrobiologia 726, 195–221. https://doi.org/10.1007/s10750-013-1764-6.
652
653 Cohen, M.C.L., de Souza, A.V., Rossetti, D.F., Pessenda, L.C.R., França, M.C., 2018. Decadal-scale
654 dynamics of an Amazonian mangrove caused by climate and sea level changes: inferences from
655 spatial-temporal analysis and Digital Elevation Models. Earth Surface Processes and Landforms 43,
656 2876–2888. https://doi.org/10.1002/esp.4440.
657
658 Cohen, M.C.L., Figueiredo, B.L., Oliveira, N.N., Fontes, N.A., França, M.C., Pessenda, L.C.R.,
659 Lima, P., 2019. Impacts of Holocene and modern sea- level changes on estuarine mangroves from
660 Northeastern Brazil. Earth Surface Processes and Landforms, esp.4737.
661 https://doi.org/10.1002/esp.4737.
662
663 Darrow, E.S., Carmichael, R.H., Calci, K.R., Burkhardt, W., 2017. Land-use related changes to
664 sedimentary organic matter in tidal creeks of the northern Gulf of Mexico. Limnol. Oceanogr. 62,
665 686–705. https://doi.org/10.1002/lno.10453.
666

667 Deines, P., 1980. The isotopic composition of reduced organic carbon, in: Fritz, P., Fontes, J.C.
668 (Eds.), Handbook of Environmental Isotope Geochemistry. The Terrestrial Environment, vol. 1. A.
669 Elsevier, Amsterdam, pp. 329–406. https://doi.org/10.1016/B978-0-444-41780-0.50015-8.
670
671 Dittmar, T., Hertkorn, N., Kattner, G., Lara, R.J., 2006. Mangroves, a major source of dissolved
672 matter sources to the oceans. Global Biogeochemical Cycles 20, GB1012.
673 https://doi.org/10.1029/2005GB002570.
674
675 Feng, J., Zhou, J., Wang, L., Cui, X., Ning, C., Wu, H., Zhu, X., Lin, G., 2017. Effects of short-term
676 invasion of Spartina alterniflora and the subsequent restoration of native mangroves on the soil
677 organic carbon, nitrogen and phosphorus stock Chemosphere 184, 774–83.
678 https://doi.org/10.1016/j.chemosphere.2017.06.060.
679
680 Feng, J., Wang, S., Wang, S., Ying, R., Yin, F., Jiang, L., Li, Z., 2019. Effects of Invasive *Spartina*
681 *alterniflora* Loisel. and Subsequent Ecological Replacement by *Sonneratia apetala* Buch.-Ham. on
682 Soil Organic Carbon Fractions and Stock. Forests 10, 171. https://doi.org/10.3390/f10020171.
683
684 Fernandes, M.E.B., Oliveira, F.P., Eyzaguirre, I.A.L., 2018. Mangroves on the Brazilian Amazon
685 Coast: Uses and Rehabilitation, in: Makowski C., Finkl C. (eds) Threats to Mangrove Forests. Coastal
686 Research Library, vol 25. Springer, Cham. https://doi.org/10.1007/978-3-319-73016-5_29.
687
688 Giri, C., Ochieng, E., Tieszen, L.L., Zhu, Z., Singh, A., Loveland, T., Masek, J., Duke, N., 2011.
689 Status and distribution of mangrove forests of the world using earth observation satellite data. Global
690 Ecol. Biogeogr. 20, 154–159. https://doi.org/10.1111/j.1466-8238.2010.00584.x.
691
692 GlobalMapper, 2017. (Version 19). Blue Marble Geographics. Hallowell, Maine, United State.
693
694 Goñi, M., Teixeira, M., Perkey, D., 2003. Sources and distribution of organic matter in
695 a river-dominated estuary (Winyah Bay, SC, USA). Estuar. Coast Shelf Sci. 57, 1023–1048.
696 https://doi.org/10.1016/S0272-7714(03)00008-8.
697
698 Gontharet, S., Mathieu, O., Lévêque, J., Milloux, M.-J., Lesourd, S., Philippe, S., Caillaud, J., Gardel,
699 A., Sarrazin, M., Proisy, C., 2014. Distribution and sources of bulk organic matter (OM) on a tropical

intertidal mud bank in French Guiana from elemental and isotopic proxies. Chemical Geology, 376, 1-10, https://doi.org/10.1016/j.chemgeo.2014.03.009.

Gorman, D., Sumida, P.Y.G., Figueira, R.C.L., Turra, A., 2020. Improving soil carbon estimates of mudflats in Araçá Bay using spatial models that consider riverine input, wave exposure and biogeochemistry. Estuarine, Coastal and Shelf Science, 238, 106734, https://doi.org/10.1016/j.ecss.2020.106734.

Grasshoff, K., Kremling, K., Ehrhardt, M., 1999. Methods of Seawater Analysis. third ed. Wiley, New York. https://doi.org/10.1002/9783527613984.

Hammer, O., Harper, D.A.T., Ryan, P.D., 2001. PAST: Paleontological statistics software package for education and data analysis. Palaeontologia Electronica 4(1): 9 pp. https://palaeo-electronica.org/2001_1/past/issue1_01.htm.

Hedges, J.I., Keil, R.G., 1995. Sedimentary organic matter preservation: an assessment and speculative synthesis. Marine Chemistry 49, 81–115. https://doi.org/10.1016/0304-4203(95)00008-F.

Hedges, J.I., Keil, R.G., Benner, R., 1997. What happens to terrestrial organic matter in the ocean? Org. Geochem. 27, 195–212. https://doi.org/10.1016/S0146-6380(97)00066-1.

Howard, J., Hoyt, S., Isensee, K., Pidgeon, E., and Telszewski, M., 2014. Coastal Blue Carbon: Methods for Assessing Carbon Stocks and Emissions Factors in Mangroves, Tidal Salt Marshes, and Seagrass Meadows, Conserv. Int. Intergov. Oceanogr. Comm. UNESCO, Int. Union Conserv. Nature, Arlington, Virginia, USA, 1–180.

ICMBio. Atlas dos Manguezais do Brasil. 2018. 1st ed. Brasília: Instituto Chico Mendes de Conservação da Biodiversidade; 176 p. https://doi.org/10.1016/S0146-6380(97)00066-1.

Jennerjahn, T.C., Ittekkot, V., 2002. Relevance of mangroves for the production and deposition of organic matter along tropical continental margins, Naturwissenschaften 89(1), 23–30. https://doi.org/10.1007/s00114-001-0283-x.

Jennerjahn, T.C., 2012. Biogeochemical response of tropical coastal systems to present and past environmental change. Earth Sci. Rev. 114, 19–41. https://doi.org/10.1016/j.earscirev.2012.04.005.

Kauffman, J.B., Bernardino, A.F., Ferreira, T.O., Giovannoni L.R., de O. Gomes L.E., Romero D.J., Jimenez L.C.Z., Ruiz F., 2018. Carbon stocks of mangroves and salt marshes of the Amazon region, Brazil. Biol. Lett. 14: 20180208. http://dx.doi.org/10.1098/rsbl.2018.0208.

Keil, R.G., Montluqon, D.B., Prahl, F.G., Hedges, J.I., 1994. Sorptive preservation of labile organic matter in marine sediments. Nature 370, 549–552. https://doi.org/

Kjerve, B., Lacerda, L.D., 1993. Mangroves of Brazil. In: Conservation and Sustainable Utilization of Mangrove Forests in Latin America and Africa Regions. Part 1: Latin America. ITTO/ISME Project PD114/90(F), pp. 245-272.

Kristensen, E., Hansen, K., 1995. Decay of plant detritus in organic-poor marine sediment: production rates and stoichiometry of dissolved C and N compounds. J. Mar. Res. 53, 675–702. https://doi: 10.1357/0022240953213115.

Kristensen, E., Bouillon, S., Dittmar, T., Marchand, C., 2008. Organic carbon dynamics in mangrove ecosystems: a review. Aquatic botany 89(2), 201-219. https://doi.org/10.1016/j.aquabot.2007.12.005.

Kusumaningtyasa, M.A., Hutahaeanc, A.A., Fischerd, H.W., Mayod, M.P., Ransbyd, D., Jennerjahn T.C., 2019. Variability in the organic carbon stocks, sources, and accumulation rates of Indonesian mangrove ecosystems. Estuarine, Coastal and Shelf Science 218, 310–323. https://doi.org/10.1016/j.ecss.2018.12.007.

Lamb, A.L., Wilson, G.P., Leng, M.J., 2006. A review of coastal palaeoclimate and relative sea-level reconstructions using $\delta^{13}C$ and C/N ratios in organic material. Earth-Sci. Reviews 75, 29–57. https://doi.org/10.1016/j.earscirev.2005.10.003.

765 Liu, D., Li, X., Emeis, K.C., Wang, Y., Richard, P., 2015. Distribution and sources of organic matter
766 in surface sediments of Bohai Sea near the Yellow River Estuary, China. Estuarine, Coastal and Shelf
767 Science 165, 128-136. https://doi.org/10.1016/j.ecss.2015.09.007.
768
769 Loring, D.H., Rantala, R.T.T., 1992. Manual for the geochemical analyses of marine sediments and
770 suspended particulate matter. Earth-Sci. Rev. 32, 235–283. https://doi.org/10.1016/0012-
771 8252(92)90001-A.
772
773 Marchio, D., Savarese, M., Bovard, B., Mitsch, W., 2016. Carbon sequestration and sedimentation in
774 mangrove swamps influenced by hydrogeomorphic conditions and urbanization in Southwest
775 Florida. Forests *7*(12), 116. https://doi.org/10.3390/f7060116.
776
777 Martorano, L.G., Pereira, L.C., Cesar, E.G.M., Pereira, I.C.B., 1993. Estudos climáticos do Estado
778 do Pará, classificação climática (Köppen) e deficiência hídrica (Thornthwhite, Mather). Belém,
779 SUDAM/EMBRAPA, SNLCS, pp. 53.
780
781 Mayer, L.M., 1994. Surface area control of organic carbon accumulation in continental shelf
782 sediments. Geochim. Cosmochim. Acta 58, 1271–1284. https://doi.org/10.1016/0016-
783 7037(94)90381-6.
784
785 McGlathery, K. J., Sundback, K., and Anderson, I. C., 2007. Eutrophication in shallow coastal bays
786 and lagoons: the role of plants in the coastal filter. Mar. Ecol. Prog. Ser. 348, 1–18.
787 https://doi/10.3354/meps07132.
788
789 Mcleod, E., Chmura, G.L., Bouillon, S., Salm, R., Björk, M., Duarte, C.M., Lovelock, C.E.,
790 Schlesinger, W.H. and Silliman, B.R., 2011. A blueprint for blue carbon: toward an improved
791 understanding of the role of vegetated coastal habitats in sequestering CO_2. Frontiers in Ecology and
792 the Environment, 9: 552-560. https://doi.org/10.1890/110004.
793
794 Meyers, P.A., 1994. Preservation of elemental and isotopic source identification of sedimentary
795 organic matter. Chem. Geol. 114, 289–302. https://doi.org/10.1016/0009-2541(94)90059-0.
796

797 Meyers, P.A., 1997. Organic geochemical proxies of paleoceanographic, paleolimnologic, and
798 paleoclimatic processes. Organic Geochemistry 27, 213 – 250. https://doi.org/10.1016/S0146-
799 6380(97)00049-1.
800

Meyers, P.A., 2003. Applications of organic geochemistry to paleolimnological econstructions: a summary of examples from the Laurentian Great Lakes. Org. Geochem. 34, 261–289. https://doi.org/10.1016/S0146-6380(02)00168-7.

Nascimento, W.R., Souza-Filho, P.W.M., Proisy, C., Lucas, R.M., Rosenqvist, A., 2013 Mapping changes in the largest continuous Amazonian mangrove belt using object-based classification of multisensor satellite imagery. Estuarine Coastal and Shelf Sci. 117, 83–93. https://doi.org/10.1016/j.ecss.2012.10.005.

Nellemann, C., Corcoran, E., Duarte, C. M., Valdrés, L., Young, C. D., Fonseca, L., Grimsditch, G., 2009. Blue Carbon - The Role of Healthy Oceans in Binding Carbon. UN Environment, GRID-Arendal. ISBN: 978-82-7701-060-1.

Paiva, R.S., Eskinazi-Leça, E., Passavante, J.Z.O., Silva-Cunha, M.G.G., Melo, N.F.A.C., 2006. Ecological considerations on phytoplankton from the Guajará bay and from the Guamá river estuary in Para, Brazil. Bol. Mus. Para. Emílio Goeldi. Ciências Naturais 1, 133–146.

Pérez, A., Machado, W., Gutierrez, D., Stokes, D., Sanders, L., Smoak, J.M., Santos, I., Sanders, C.J., 2017. Changes in organic carbon accumulation driven by mangrove expansion and deforestation in a New Zealand estuary. Est. Coast. Shelf Sci. 192, 108–116. https://doi.org/10.1016/j.ecss.2017.05.009.

Pérez, A., Libardoni, B.G., Sanders, C.J., 2018. Factors influencing organic carbon accumulation in mangrove ecosystems. Biol. Lett. 14 (10). https://doi.org/10.1098/rsbl. 2018.0237.

Peterson, B.J., Howarth, R.W., 1987. Sulfur, carbon, and nitrogen isotopes used to trace organic matter flow in the salt- marsh estuaries of Sapelo Island, Georgia. Limnology and oceanography 32(6), 1195-1213. https://doi.org/10.4319/lo.1987.32.6.1195.

Prahl, F.G., De Lange, G.T., Scholten, S., Cowie, G.L., 1997. A case of post-depositional aerobic degradation of terrestrial organic matter in turbidite deposits from the Madeira Abyssal Plain. Org. Geochem. 27, 141–152. https://doi.org/10.1016/S0146-6380(97)00078-8.

Prasad, M.B.K., Kumar, A., Ramanathan, A.L., Datta. D.K., 2017. Sources and dynamics of sedimentary organic matter in Sundarban mangrove estuary from Indo-Gangetic delta. Ecological Processes 6, 8. https://doi.org/10.1186/s13717-017-0076-6.

Prasad, M.B.K., Ramanathan, A.L., 2009. Organic matter characterization in a tropical estuarine-mangrove ecosystem of India: preliminary assessment by using stable isotopes and lignin phenols. Estuarine Coastal Shelf Science 84(4): 617–624. https://doi.org/10.1016/j.ecss.2009.07.029.

Ranjan, R.K., Routh, J., Ramanathan, A.L., Klump, J.V., 2011. Elemental and stable isotope records of organic matter input and its fate in the Pichavaram mangrove–estuarine sediments (Tamil Nadu, India). Marine Chemistry 126, 163–172. https://doi.org/10.1016/j.marchem.2011.05.005.

Ray, R., Majumder N., Das, S., Chowdhury, C., Jana, T.K., 2014. Biogeochemical cycle of nitrogen in a tropical mangrove ecosystem, east coast of India. Marine Chemistry, 167, 33–43. https://doi.org/10.1016/j.marchem.2014.04.007.

Ray, R., Majumder, N., Chowdhury, C., Das, S., Jana, T.K., 2017. Phosphorus Budget of the Sundarban Mangrove Ecosystem: Box Model Approach. Estuaries and Coasts 41, 1036–1049. https://doi.org/10.1007/s12237-017-0332-0.

Routh, J., Meyers, P.A., Choudhury, P., Kumar, B., 2009., A sediment record of recent nutrient loading and trophic state change in Lake Norrviken, Sweden. J. Paleolimnol. 42, 325–341. https://doi.org/10.1007/s10933-008-9279-2.

Redfield, A.C., Ketchum, B.H. and Richards, F.A., 1963. The influence of organisms on the composition of sea-water, in: Hill, M.N. (Ed.) The composition of seawater: Comparative and descriptive oceanography. The sea: ideas and observations on progress in the study of the seas, 2: pp. 26-77.

Rosentreter, J.A., Maher, D.T., Erler, D.V., Murray, R., Eyre, B.D., 2018. Seasonal and temporal CO_2 dynamics in three tropical mangrove creeks – a revision of global mangrove CO_2 emissions. Geochim. Cosmochim. Acta 222, 729–745. https://doi.org/10.1016/j.gca.2017.11.026.

Saintilan, N., Rogers, K., Mazumder, D., Woodroffe, C., 2013. Allochthonous and autochthonous contributions to carbon accumulation and carbon store in southeastern Australian coastal wetlands. Estuar. Coast Shelf Sci. 128, 84–92. https://doi.org/10.1016/j.ecss.2013.05.010.

Sanders, C.J., Santos, I.R., Maher, D.T., Breithaupt, J.L., Smoak, J.M., Ketterer, M., Call, M., Sanders, L.M., Eyre, B.D., 2016. Examining $^{239+240}$Pu, ^{210}Pb and historical events to determine carbon, nitrogen and phosphorus accumulation in mangrove sediments of Moreton Bay, Australia. J. Environ. Radioact. 151, 623–629. https://doi.org/10.1016/j.jenvrad.2015.04.018.

Santos, I.R., Maher, D.T., Larkin R., Webb, J.R., Sanders, C.J., 2019. Carbon outwelling and outgassing vs. burial in an estuarine tidal creek surrounded by mangrove and saltmarsh wetlands. Limnol. Oceanogr. 64, 996–1013. https://doi.org/10.1002/lno.11090.

Sasmito, S.D., Kuzyakov, Y., Lubis, A.A., Murdiyarso, D., Hutley, L.B., Bachri, S., Friess, D.A., Martius, C., Borchard, N. 2020. Organic Carbon Burial and Sources in Soils of Coastal Mudflat and Mangrove Ecosystems. Catena, 187, 104414. https://doi.org/10.1016/j.catena.2019.104414.

Schultz, D.J., Calder, J.A., 1976. Organic carbono ^{13}C/^{12}C variations in estuarine sediments. Geochim. Cosmochim. Acta 40, 381–385. https://doi.org/10.1016/0016-7037(76)90002-8.

Silva, C.A., Souza-Filho, P.W.M., Rodrigues, S.W.P., 2009. Morphology and modern sedimentary deposits of the macrotidal Marapanim Estuary (Amazon, Brazil). Continental Shelf Research 29, 619–631. https://doi.org/10.1016/j.csr.2008.09.018.

Smoak, J.M., Breithaupt, J.L., Smith, T.J., Sanders, C.J., 2013. Sediment accretion and organic carbon burial relative to sea-level rise and storm events in two mangrove forests in Everglades National Park. Catena 104, 58-66.

Steinmuller, H.E., Foster, T.E., Boudreau, P., Ross Hinkle, C., Chambers, L.G., 2020. Tipping Points in the Mangrove March: Characterization of Biogeochemical Cycling Along the Mangrove–Salt Marsh Ecotone. Ecosystems 23, 417–434. https://doi.org/10.1007/s10021-019-00411-8.

Udden, J.A., 1914. Mechanical composition of clastic sediments. Bulletin of the Geological Society of America 25, 655–744.

Vilhena, M.P.S.P., Costa, M.L., Berrêdo, J.F., 2013. Accumulation and transfer of Hg, As, Se, and other metals in the sediment-vegetation-crab-human food chain in the coastal zone of the northern Brazilian state of Para (Amazonia). Environ Geochem Health, 35, 477–494. https://doi.org/10.1007/s10653-013-9509-z.

Vilhena, M.P.S.P., Costa, M.L., Berrêdo, J.F., Paiva, R.S., Moreira M.Z., 2018. The sources and accumulation of sedimentary organic matter in two estuaries in the Brazilian Northern coast. Regional Studies in Marine Science 18, 188–196. https://doi.org/10.1016/j.rsma.2017.10.007.

Watanabe, K., Kuwae, T., 2015. How organic carbon derived from multiple sources contributes to carbon sequestration processes in a shallow coastal system? Global Change Biol. 21, 2612–2623. https://doi.org/10.1111/gcb.12924.

Wentworth, C.K., 1922. A scale of grade and class terms for clastic sediments. Journal of Geology 30, 377–392.

Zonneveld, K.A.F., Versteegh, G.J.M., Kasten, S., Eglinton, T.I., Emeis, K.-C., Huguet, C., Koch, B.P., de Lange, G.J., de Leeuw, J.W., Middelburg, J.J., Mollenhauer, G., Prahl, F., Rethemeyer, J., Wakeham, S., 2010. Selective preservation of organic matter in marine environments; processes and impact on the fossil record. Biogeosciences 7, 483–511. https://doi.org/10.5194/bg-7-483-2010.

Figure Captions

Fig. 1. (A) and (B) Map of the study area in Marapanim estuarine mangrove, Brazil. (B) Sampling location (P1, P2 and P3). (C) Catchment and mudflat areas related to the sampling sites. (D) Digital vegetation height model. (E) The diagrammatic mangrove forest distribution and positioning of the sampled cores in the mud tidal flat mangrove sediments. Black dashed lines represent the height of the mangrove.

Fig. 2. $\ln^{210}Pb_{ex}$ (Bq kg^{-1}) activities versus depth in the sediment cores (P1, P2 and P3), sedimentation rates were calculated using selected points of $^{210}Pb_{ex}$ profiles (filled symbols). Open symbols correspond to result interpreted as biologically and physically disturbed.

Fig. 3. Depth profiles of grain size, DBD, TOC, TN, TP, $\delta^{15}N$, $\delta^{13}C$ and TOC/TN (molar ratio) for the sediment cores (P1, P2 and P3). Including proportions of terrestrial (OM_{terr}) and marine (OM_{mar}) sedimentary OM, during wet (filled circles) and dry (open circles) seasons.

Fig. 4. (a) Principal Component Analysis (PCA) plot showing the multivariate variation among three sites in terms of environmental variables. (b) Vectors indicate the direction and strength of each environmental variable to the overall distribution. The first two principal axes explained 74.5 % of the variance.

Fig. 5. TOC, TN and TP stocks (solid bars, g m^{-2}) and accumulation rates (striped bars, g m^{-2} yr^{-1}) in the sediment cores (P1, P2 and P3). The error bars are based on the standard deviation from the average between the wet and dry season dataset.

Fig. 6. Origin of sedimentary OM as indicated by $\delta^{13}C$ against TOC/TN (molar ratio). Fields are defined from the compilation of coastal sediments by Lamb et al. (2006). The phytoplankton (white diamond symbol) and Mangrove plants (black diamond symbol) endmember data are taken from the original data in this study.

Fig. 7. Schematic comparing the global carbon (Perez et al., 2018) and nitrogen and phosphorus burial rates (Breithaupt et al. 2014) for conserved mangrove forest with Marapanim mangrove creek (this study) and the global mangrove water-atmosphere CO_2 and CH_4 flux rates (Rosentreter et al., 2018) with ‘‘Furo do Meio” mangrove creek (Call et al. 2019). All rates are in g m^{-2} yr^{-1}.

Figure 1

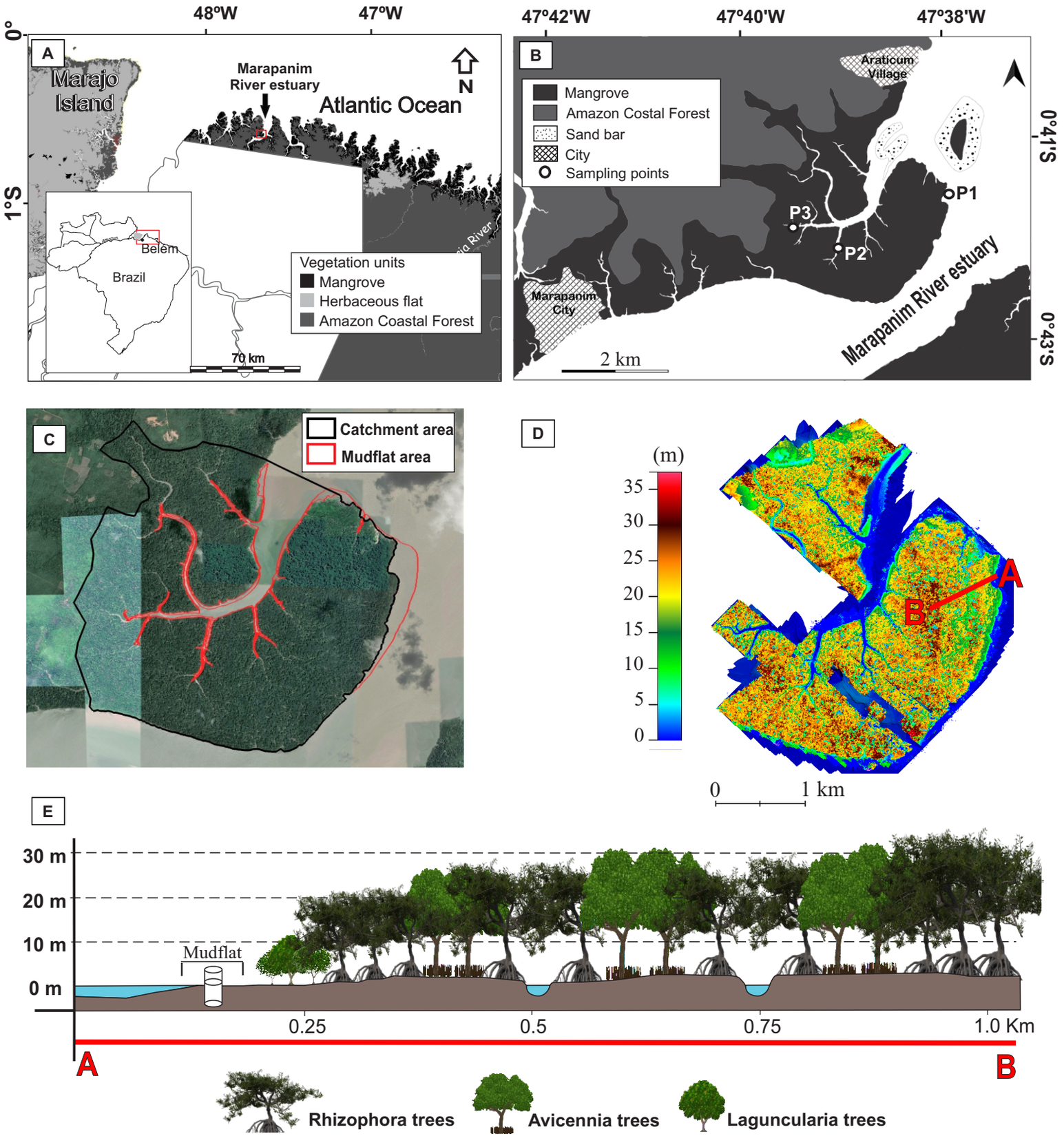
A
Marajo Island
Marapanim River estuary
Atlantic Ocean
N
48°W
47°W
0°
1°S
Belém
Brazil
70 km
Vegetation units
Mangrove
Herbaceous flat
Amazon Coastal Forest
B
47°42'W
47°40'W
47°38'W
0°41'S
0°43'S
Araticum Village
Mangrove
Amazon Costal Forest
Sand bar
City
Sampling points
P1
P2
P3
Marapanim City
Marapanim River estuary
2 km
C
Catchment area
Mudflat area
D
(m)
35
30
25
20
15
10
5
0
A
B
0
1 km
E
30 m
20 m
10 m
0 m
Mudflat
0.25
0.5
0.75
1.0 Km
A
B
Rhizophora trees
Avicennia trees
Laguncularia trees

Figure 2

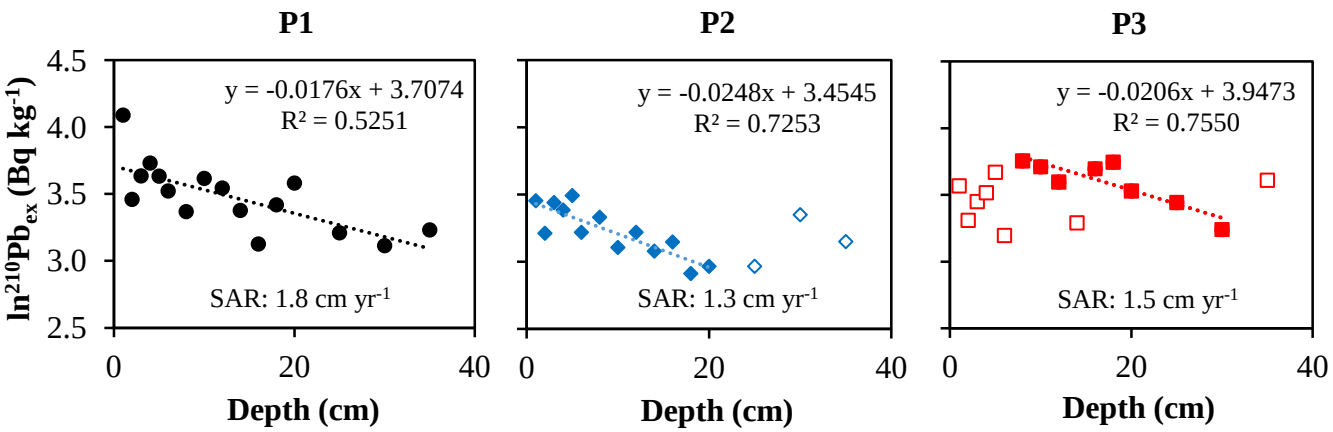
P1
P2
P3
y = -0.0176x + 3.7074
R² = 0.5251
y = -0.0248x + 3.4545
R² = 0.7253
y = -0.0206x + 3.9473
R² = 0.7550
SAR: 1.8 cm yr-1
SAR: 1.3 cm yr-1
SAR: 1.5 cm yr-1
ln210Pbex (Bq kg-1)
4.5
4.0
3.5
3.0
2.5
0
20
40
Depth (cm)

Figure 3

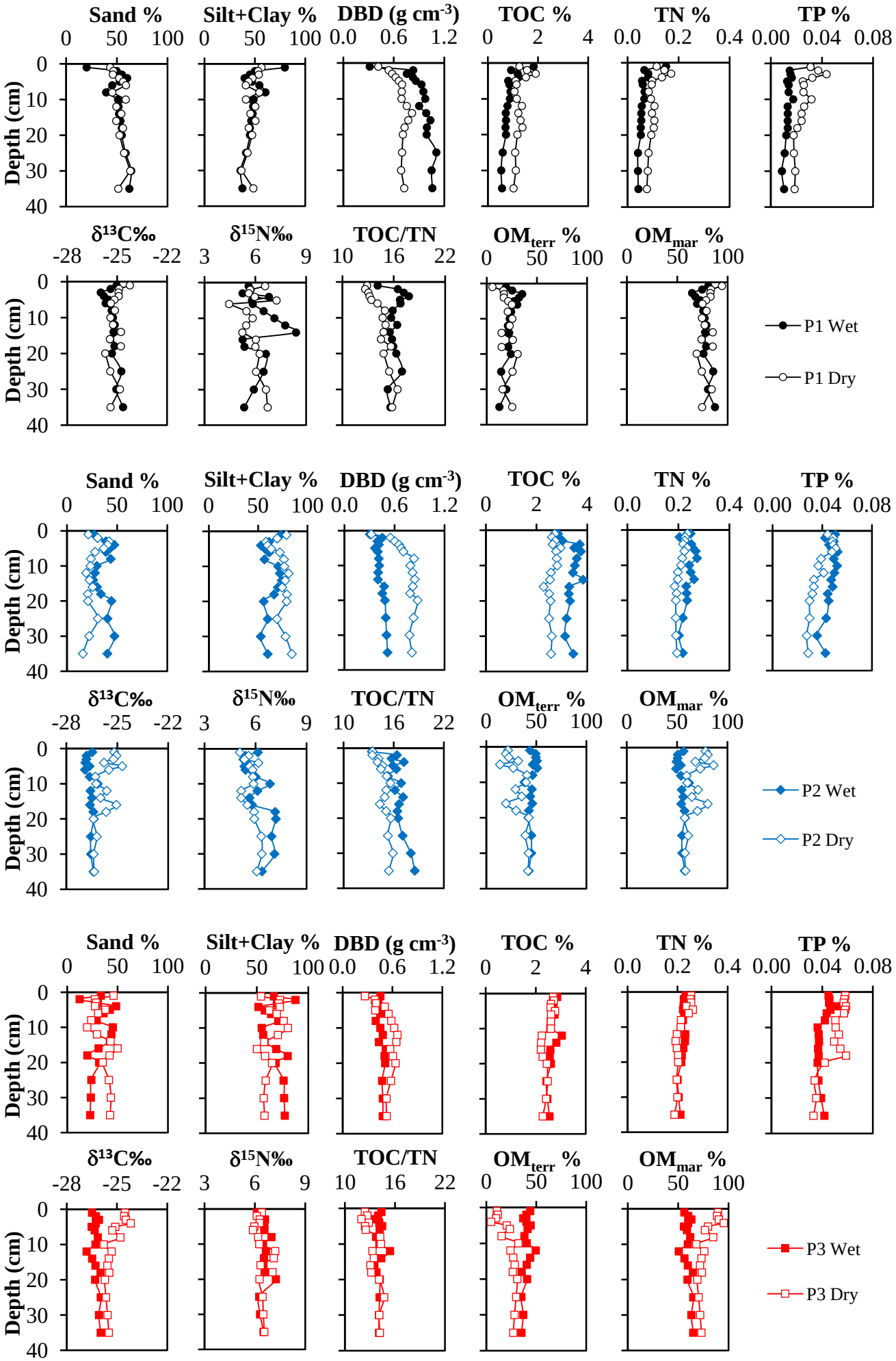
Sand %
Silt+Clay %
DBD (g cm-3)
TOC %
TN %
TP %
δ13C‰
δ15N‰
TOC/TN
OMterr %
OMmar %
Depth (cm)
P1 Wet
P1 Dry
P2 Wet
P2 Dry
P3 Wet
P3 Dry

Figure 4

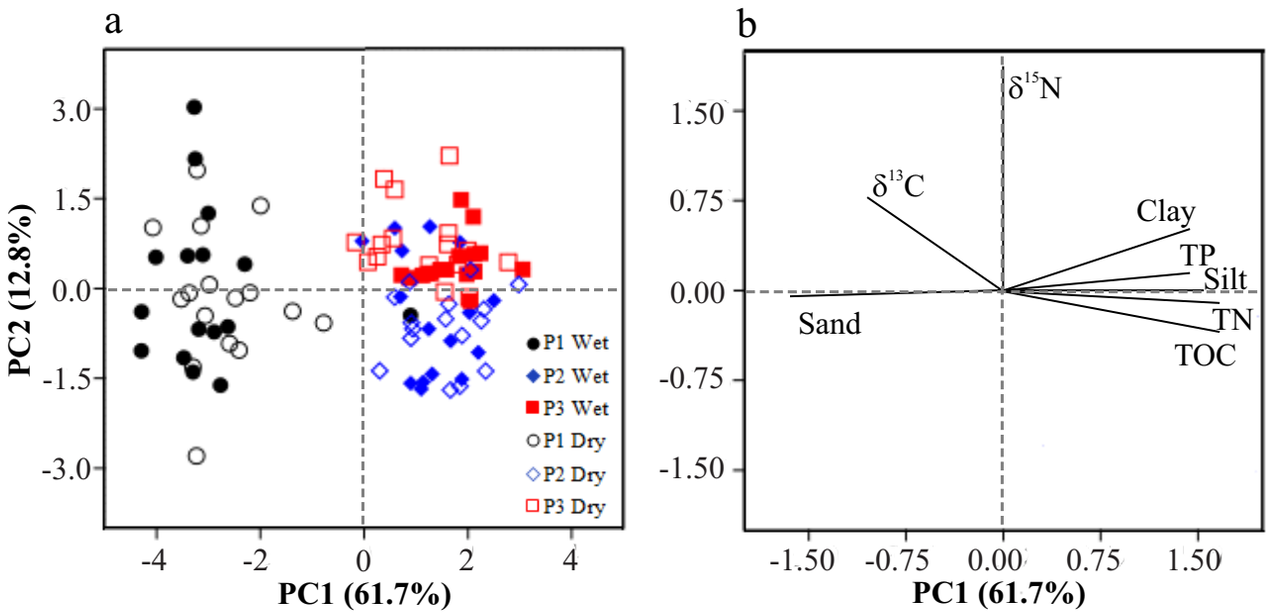
a
3.0
1.5
0.0
-1.5
-3.0
PC2 (12.8%)
-4
-2
0
2
4
PC1 (61.7%)
P1 Wet
P2 Wet
P3 Wet
P1 Dry
P2 Dry
P3 Dry
b
1.50
0.75
0.00
-0.75
-1.50
δ15N
δ13C
Clay
TP
Silt
TN
TOC
Sand
-1.50
-0.75
0.00
0.75
1.50
PC1 (61.7%)

Figure 5

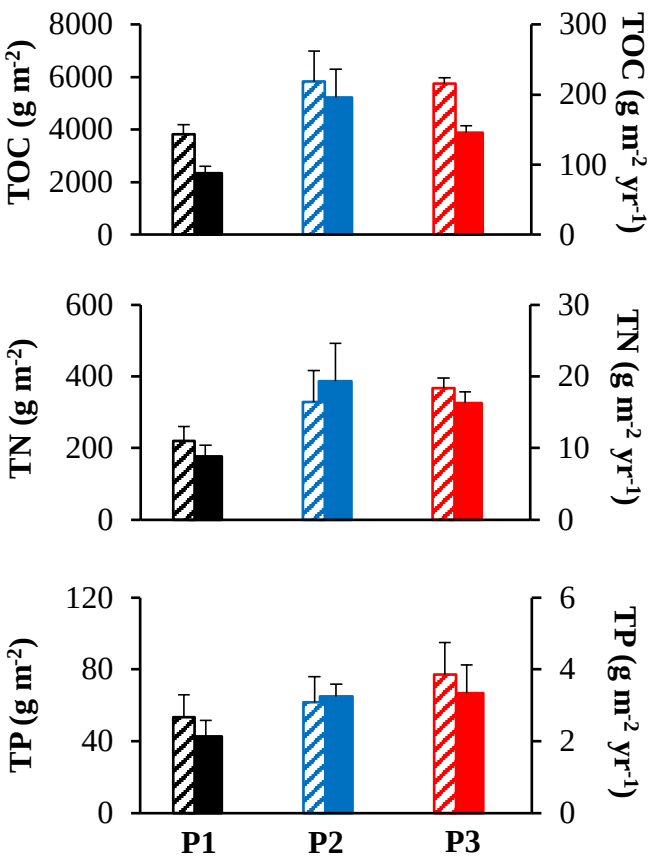
TOC (g m-2)
8000
6000
4000
2000
0
300
200
100
0
TOC (g m-2 yr-1)
TN (g m-2)
600
400
200
0
30
20
10
0
TN (g m-2 yr-1)
TP (g m-2)
120
80
40
0
6
4
2
0
TP (g m-2 yr-1)
P1
P2
P3

Figure 6

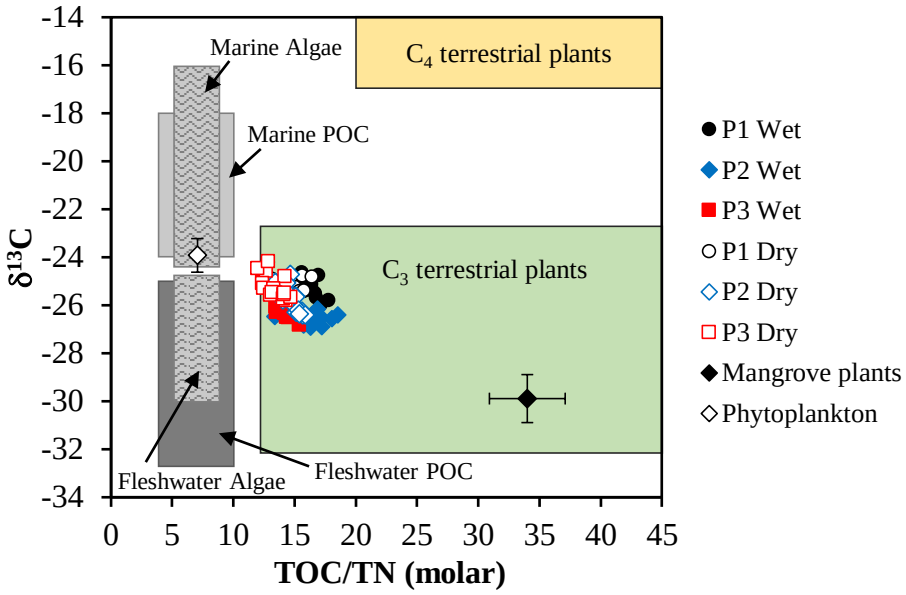
-14
-16
-18
-20
-22
-24
-26
-28
-30
-32
-34
δ13C
0
5
10
15
20
25
30
35
40
45
TOC/TN (molar)
Marine Algae
Marine POC
C4 terrestrial plants
C3 terrestrial plants
Fleshwater Algae
Fleshwater POC
P1 Wet
P2 Wet
P3 Wet
P1 Dry
P2 Dry
P3 Dry
Mangrove plants
Phytoplankton

Figure 7

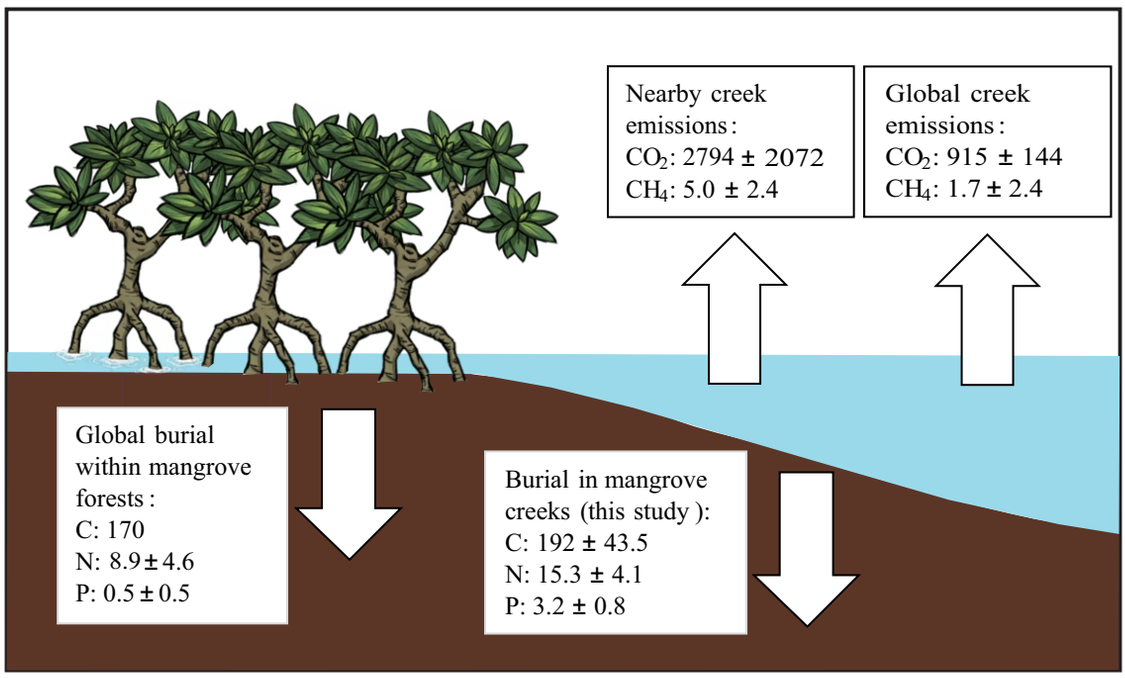
Nearby creek emissions:
CO_2: 2794 ± 2072
CH_4: 5.0 ± 2.4
Global creek emissions:
CO_2: 915 ± 144
CH_4: 1.7 ± 2.4
Global burial within mangrove forests:
C: 170
N: 8.9 ± 4.6
P: 0.5 ± 0.5
Burial in mangrove creeks (this study):
C: 192 ± 43.5
N: 15.3 ± 4.1
P: 3.2 ± 0.8